How to cite: *Angew. Chem. Int. Ed.* **2024**, *63*, e202403792
doi.org/10.1002/anie.202403792

Drug Discovery

Nanomole Scale Screening of Fluorescent RNA-Methyltransferase Probes Enables the Discovery of METTL1 Inhibitors

*J. Laurenz Meidner[+], Ariane F. Frey[+], Robert A. Zimmermann[+], Mark O. Sabin, Zarina Nidoieva, Annabelle C. Weldert, Sabrina N. Hoba, Mackenzie W. Krone, and Fabian Barthels**

Abstract: RNA methylation is a metabolic process validated for its association with various diseases, and thus, RNA methyltransferases (MTases) have become increasingly important in drug discovery. Yet, most frequently utilized RNA MTase assays are limited in their throughput and hamper this rapidly evolving field of medicinal chemistry. In this study, we describe a modular nanomole scale building block system that allowed the identification of tailored fluorescent MTase probes to unlock a broad selection of MTase drug targets for fluorescence-based binding assays. Probe candidates were initially prepared on a 4 nanomole scale and could be tested directly from crude reaction mixtures to allow rapid probe identification and optimization. Using an alkyne-azide click late-stage functionalization strategy and in silico protein databank mining, we established a selection of fluorescent probes suitable for relevant drug targets from the METTL and NSUN families, as well as bacterial and viral MTases. Using this concept, a high-throughput screening on the unexplored drug target METTL1 discovered three hit compounds with micromolar potency providing a (1*H*-pyrazol-4-yl)pyridine-based starting point for METTL1 drug discovery.

RNA has become increasingly important in modern drug discovery as a drug itself, a target for drugs, and not at last a key component in cellular pathways associated with malignancies and infections.[3,4] In this regard, methylation of RNA is a metabolic process in many organisms validated for their association with various diseases.[5] With STC-15, the first-in-class RNA methyltransferase (MTase) inhibitor targeting METTL3/14 was brought into clinical trials just in 2023 highlighting the recent shift of paradigm.[6] During the preparation of this manuscript, the discovery of a series of small-molecule inhibitors of METTL1 was reported by Nai et al.[7]

Currently, enzymatic scintillation assays using ^{3}H-labelled *S*-adenosylmethionine (SAM) and the LC/MS-based detection of the MTase reaction co-product *S*-adenosylhomocysteine (SAH) are the state-of-the-art for screening drug candidates on RNA MTases such as METTL3/14,[8] DNMT2,[1] NSUN2,[9] and anti-infective targets like *H. influenzae* TrmD or SARS-CoV2 nsp10/16.[10,11] Such enzyme activity-based assay formats are valuable for the determination of inhibitory constants (IC_{50}, K_I) of advanced drug- and lead-like candidates but have significant drawbacks compared to biophysical ligand binding assays such as increased susceptibility to assay interference and poor reproducibility at high ligand concentrations.[12] Despite these limitations, time consumption and reagent/instrument costs of current activity-based and biophysical MTase assays are inherently high, thus, limiting the application for medium- to high-throughput applications and hampering this steadily evolving field of medicinal chemistry.[13]

To tackle this methodological gap, we recently introduced a fluorescent probe for screening DNMT2 inhibitors using microscale thermophoresis (MST) and fluorescence polarisation (FP) assays.[14] The 5-FAM-triazolyl-adenosyl-diaminobutyric acid (**FTAD**) probe binds to DNMT2's active site where it is displaced by ligands such as drug candidates, offering a convenient primary assay for drug screening. Compared to label-free screening methods such as SPR (Surface plasmon resonance) or ITC (Isothermal titration calorimetry), this active site probe shows a major advantage over the previous methods for MTase drug screening applications. Allosteric non-inhibiting binders are not detected, as these do not influence the catalytic MTase function and are mostly false-positive hits in terms of inhibitor development. Yet, this concept shows its severe limitation for usage with numerous other RNA MTases e.g., from the NSUN-, and METTL-families, as well as non-Rossmann-fold MTases such as bacterial TrmD, because **FTAD** shows only weak protein binding affinity ($K_D >$ 20 μM) to many of those disease-associated potential drug targets (Figure S1 A).

[*] J. L. Meidner,[+] A. F. Frey,[+] Dr. R. A. Zimmermann,[+] M. O. Sabin, Dr. Z. Nidoieva, A. C. Weldert, S. N. Hoba, Dr. F. Barthels
Institute of Pharmaceutical and Biomedical Sciences
Johannes Gutenberg-University, 55128 Mainz, Germany.
E-mail: barthels@uni-mainz.de
Dr. M. W. Krone, Dr. F. Barthels
Department of Molecular, Cellular, and Developmental Biology
Yale University, New Haven, CT 06511, USA.
[+] Authors have contributed equally.

In this current study, we describe a modular building block system using combinational nanomole-scale chemistry that allowed us to identify tailored fluorescent probes consisting of two recombined segments (a fluorophore & an MTase recruiter), to unlock a much broader selection of MTase targets for drug discovery including previously untargeted MTases from the NSUN- and METTL-families (Figure 1). Subsequently, we have shown the general usability of this system for a drug screening application of the untargeted MTase METTL1 (Figure 5).

In the first step of our probe development campaign, we considered SAH-triazole-derived chemotypes as probe candidates because a.) the SAH-triazole motif is well established among MTase inhibitors,[−15–17] and b.) we could rapidly employ a selection of diverse fluorophore azides to be attached to the existing SAH-alkyne building block by copper-catalyzed alkyne-azide click (CuAAC) late-stage functionalization reaction. To cover a broad spectrum of physicochemical fluorophore properties, we utilized fluorophore azides which can be categorized into three groups: globular dyes, like 5-FAM, Atto488, Atto590, and Atto647N; small organic fluorophores like NBD or BODIPY; and cyanine-type elongated fluorophores like Cy3/Cy5. From a physicochemical view, this set of fluorophores can also be characterized by molecular charge (from Atto488: X^{-1} to Atto590: X^{+1}) or hydrophobicity (NBD: most polar, Cy5: least polar). While all of our selected fluorophore azides are biocompatible and show similar suitability for MST- resp. FP-based assays, it is noteworthy that when selecting your fluorophores, those that do not have a flexible linker ("propeller effect") and whose fluorescence lifetime is short (<10 ns) are best suited to develop FP assays.[18] For initial probe screening, the probe synthesis was conducted on a 4 nanomole scale (416 µM in 12 µL) according to conventional CuAAC conditions with Cu(II), ascorbate, and tris((1-benzyl-4-triazolyl)methyl)amine in 1:1 DMSO/water (Figure 2A).[2]

Afterward, the success of the reaction was verified by LC/MS. The reaction was considered successful if a product conversion of >85 % was achieved (Figure S5), and hence, the probes could be tested directly from the crude reaction mixture by an MST displacement experiment with the natural ligand SAH (Figure 2B).[14] Importantly, we ensured that the CuAAC additives did not interfere with the MST assay by validating the MST binding characteristics of in situ synthesized **FTAD** vs. HPLC-purified **FTAD** as indistinguishable (Figure S1B,C). Subsequently, these probe candidates were screened on two selected model MTases, METTL1 and NSUN6, for which currently no selective inhibitors are available, while overexpression was found to drive oncogenesis, rendering these enzymes potential, yet unexplored, drug targets.[19,20] For primary probe screening, an MTase solution (2 µM) was treated with the respective probe candidate (100 nM), and the thermophoresis profile was acquired both with or without the addition of the active site ligand SAH (100 µM). The probe with the largest MST shift between the presence of SAH and without this competitor was considered a promising probe candidate. During this probe screening, for METTL1 (Figure 2C) and NSUN6 (Figure S2A), two BODIPY- resp. Cy5-containing probes were identified. Subsequently, these probes were resynthesized, purified, and validated on a preparative scale.

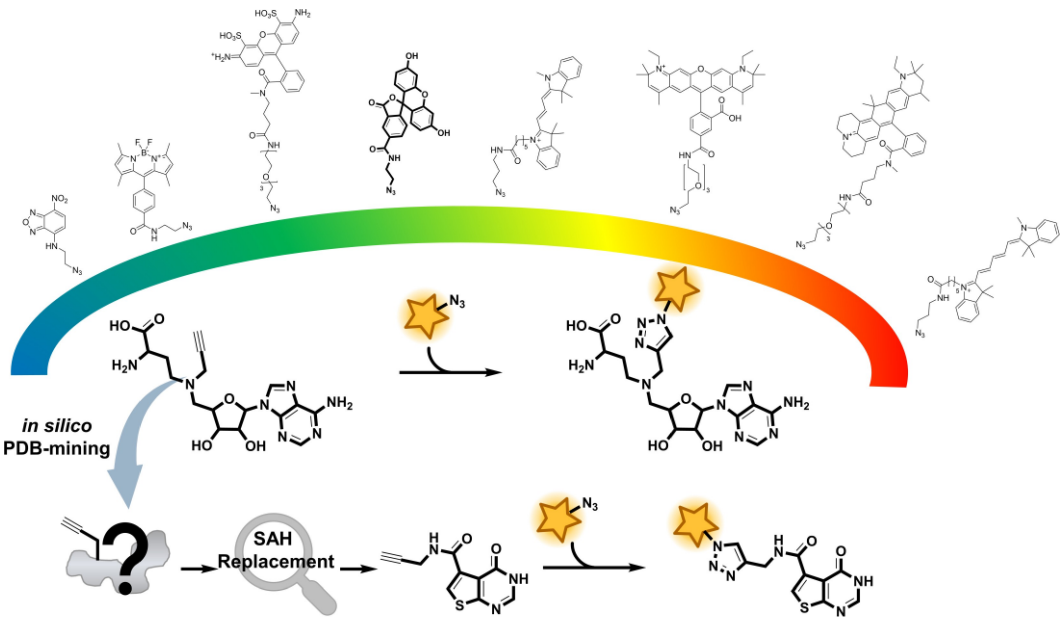

Figure 1. Overview of the nanomole-scale strategy for the development of MTase probes. Eight diverse fluorophore azides (represented as stars) were attached to a SAH-alkyne building block by CuAAC late-stage functionalization reactions.[1,2] By this, probe candidates were prepared on a 4 nanomole scale and tested directly from crude reaction mixtures for target affinity. Secondly, the variation of the SAH-core structure by a protein databank (PDB)-mining allowed the identification of eleven SAH-replacement scaffolds that were also introduced to fluorophore functionalization to expand the chemical space of MTase probes. This strategy led to the identification of a thienopyrimidine probe suitable for SPOUT-fold bacterial MTases which did not bind the SAH-alkyne building block.

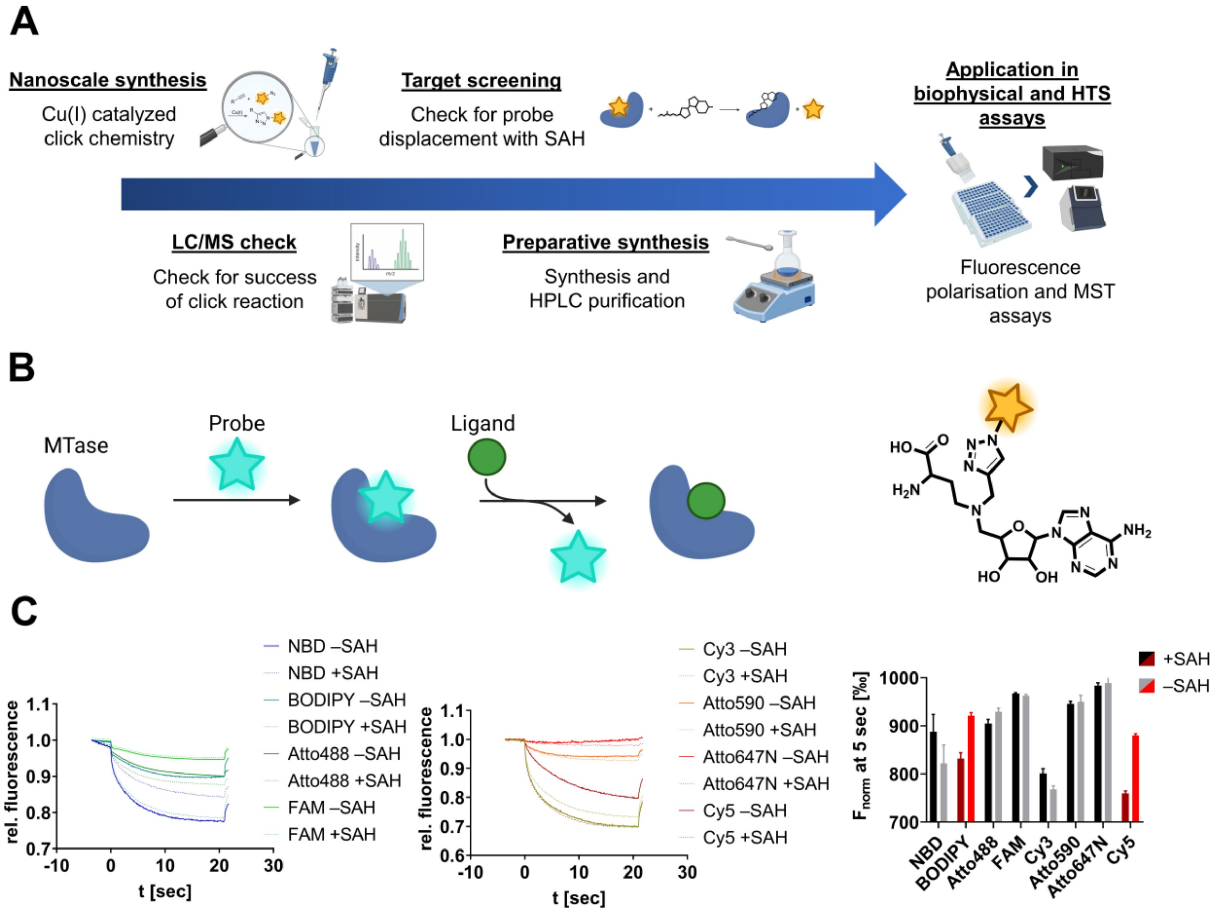

Figure 2. MTase probe development strategy. (**A**) Fluorescent probe development was achieved in five sequential steps. (**B**) Schematic depiction of the displacement assay: Functional probes form complexes with MTases, and thus, the thermophoresis (MST assay) or polarisation (FP assay) is altered compared to the unbound probe. Titration with a competitive ligand (such as SAH) leads to the displacement of the probe and restores the initial unbound fluorescence properties. (**C**) Screening results of TAD-probe candidates (100 nM) on METTL1 (2 μM) by displacement MST assays. The MST traces (**left**) in the presence of SAH (100 μM) or without the SAH competitor yielded MST shifts (**right**) revealing Cy5-TAD displays the largest SAH-induced shift (ΔF_{norm} at 5 sec), thus, rendering this probe a promising probe candidate for METTL1 (mean ± SD, $n = 3$).

By this, it turned out that **Cy5TAD** is well suitable for probing METTL1 (Figure 4A) and NSUN6 (Figure S3A), while BODIPY-TAD was found to be unstable in buffer due to spontaneous deborylation.

Also, we applied the newly discovered TAD probes to the homologous NSUN2 and METTL3/14: two cancer targets for which few inhibitors have been developed lately, but no probe or biophysical screening assay has been reported yet.[8,9,21] Here, **Cy5TAD** (NSUN2) and **FTAD** (METTL3/14) were found to be effective probes, respectively (Figure S3).

As a next step, we aimed to assay the newly discovered probes on MTases outside of the NSUN- and METTL families. Hence, to develop a suitable probe for a drug-relevant bacterial MTase, we performed analogous MST displacement screenings on the pathogen-associated MTase *H. inf.* TrmD, which is known for its unique SPOUT-fold binding mode of the SAM cofactor.[10] Initially, no TAD-probe candidate with a significant MST shift could be identified (Figure S2B). We hypothesized that the SAH-triazole (TAD) chemotype is not suitable for non-Rossmannfold MTases. To address this issue, we designed a strategy to vary the MTase recruiter part to obtain SAH replacements that are suitable for a more diverse set of MTases (Figure 1). To establish SAH-replacement scaffolds, we followed a protein databank (PDB) mining strategy (details and code in SI). Principally, we established a chemoinformatic pipeline that searches the PDB for SAH-binding pockets in which only chemically dissimilar non-SAH-like ligands are bound (Figure 3A).

Clustering of the results yielded eleven SAH replacement lead scaffolds **1**–**11**, which can be implemented for CuAAC functionalization and probe screening (Figure 3B). With this expanded set of alkynes, analogous nanomole-scale coupling to 5-FAM-N_3 resp. Cy5-N_3 and subsequent MST displacement assays were performed, yielding a thienopyrimidine probe (**Cy5TPD**) which was found to be suitable for probing TrmD in MST and FP assays (Figure 4C). Validation on a preparative scale was accomplished for all three probes (**FTAD**, **Cy5TAD**, and **Cy5TPD**) which were effective on this investigated set of MTase targets (Figure 4A–C). For biophysical characterization, we deter-

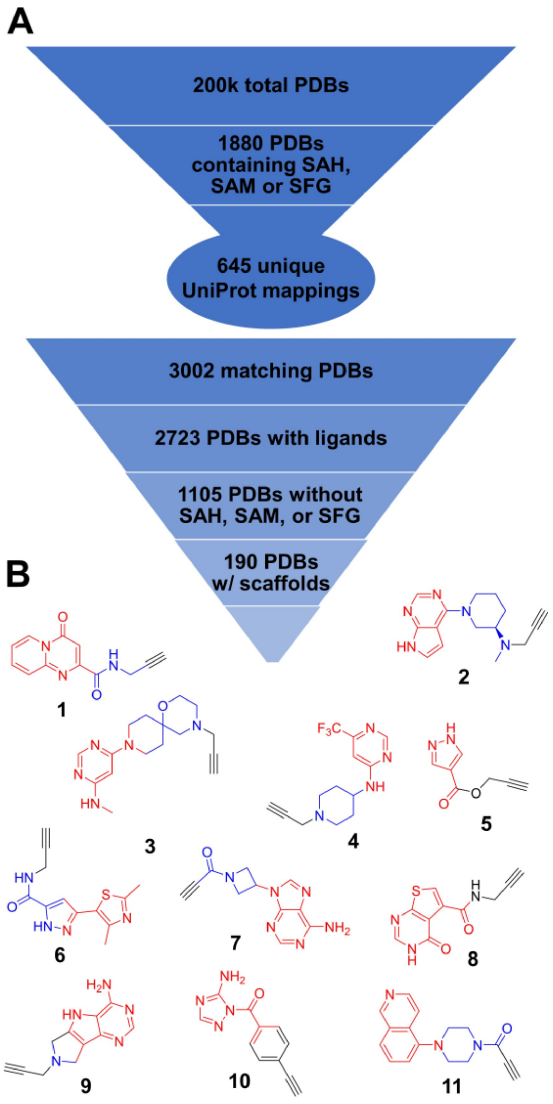

Figure 3. Description of the PDB-mining strategy. (**A**) Cheminformatic pipeline for the search of non-SAH scaffolds binding to SAH-pockets in crystallographic PDB structures. (**B**) Clustering of 190 ligands revealed eleven SAH-replacement alkyne **1**–**11** suitable for CuAAC functionalization. Red: adenine replacement; blue: ribose replacement; black: alkyne handle (see Figure S4 for crystallographic ligand poses).

mined probe-target binding affinities by MST/FP assays, as well as SAH affinities by preparative displacement assays which were agreeing with the ITC-derived SAH binding affinities (Table 1, Figure S6).

Also, we could confirm that protein binding of all three probes leads only to a minimal change in the fluorescence quantum yield. By this, we assured that local changes in fluorescence levels are not distorting apparent fluorescence polarisation values (Figure S7). Furthermore, we have worked on a structural rationale to predict which probe is suitable for a particular MTase. Two factors were found decisive in the choice of a functional probe: The conformation of the SAH molecule in the crystal structure and the flexibility of the MTase binding pocket determined by crystallographic B'-factors (Table S1).[22] If a crystal structure is available, a suitable probe can be chosen using a decision tree (Figure 4E). First, MTases that have bound a kinked SAH ligand (<100°) might not be suitable for the two TAD probes, so in this case, the Cy5-TPD probe should be used (Figure 4D). Secondly, MTases with greater flexibility (B'>0) in the binding pocket enable the use of **FTAD**, whereas MTases with more rigid binding pocket elements prefer **Cy5TAD** (Table S1).

Table 1: Characterization of fluorescent MTase probes by MST/FP-assays (mean ± SD, $n=3$).

MTase	Probe	Probe K_D by FP [μM]	Probe K_D by MST [μM]	SAH K_D FP/MST [μM]	SAH K_D by ITC [μM]
DNMT2	FTAD	6.4 ± 0.7	2.1 ± 0.1	13.6 ± 2.3	13.6 ± 4.4[a]
NSUN2	Cy5TAD	2.4 ± 0.5	6.9 ± 0.3	7.9 ± 0.6	4.7 ± 0.8
NSUN6	Cy5TAD	6.4 ± 0.6	6.5 ± 1.0	4.5 ± 1.1	4.2 ± 0.2
METTL1	Cy5TAD	1.6 ± 0.3	3.2 ± 0.2	1.6 ± 0.1	3.1 ± 0.1
METTL3/14	FTAD	1.1 ± 0.1	1.1 ± 0.1	3.1 ± 0.7	3.7 ± 0.1[a]
***H. inf.* TrmD**	Cy5TPD	2.0 ± 0.7	1.3 ± 0.3	13.9 ± 1.7	9.2 ± 0.4
SARS-CoV2 nsp10/16	FTAD	n.d.	1.2 ± 0.1	4.2 ± 0.9	5.7 ± 1.9[a]

[a] Value determined in the literature.[1,25,26]

Finally, we utilized the newly identified **Cy5TAD** probe for a high-throughput drug screening on the largely unexplored cancer drug target METTL1, which introduces the m^7G modifications to various tRNAs.[20] Using an FP assay screening setup, we have tested an in-house library of 2230 drug-like candidates to identify initial binding scaffolds suitable for subsequent lead optimization (Figure 5).

The drug candidate library was added to a master mix of recombinantly expressed METTL1 protein (1 μM), the **Cy5TAD** probe (20 nM), and a final drug compound concentration of 200 μM (Figure 5A). Compounds that displaced the **Cy5TAD** probe by at least 50 % (<20 mP) and did not interfere with the fluorescence properties of the probe were defined as screening hits (see details of screening setup and hit selection in the SI).

By this, we identified three hit compounds with micromolar potency which could be also validated by orthogonal biophysical (ITC, FP, SPR) and enzymatic METTL1 assays (Figure 5D–I). Among those hits, (*S*)-crizotinib was found to be the most promising starting point to kick-off drug discovery on METTL1 as it showed binding during FP (K_D = 138 μM), ITC (K_D = 177 μM), SPR (K_D = 178 μM), and enzyme inhibition (IC_{50} = 158 μM) in all biophysical and enzymatic ^{3}H-experiments. Of note, (*S*)-crizotinib did not bind or inhibit any of the other RNA MTases at ligand concentrations as high as 1 mM (Figure 5C), rendering this compound a METTL1 selective HTS hit. Interestingly, the corresponding kinase inhibiting eutomer (*R*)-crizotinib (marketed as Xalkori) did not bind to METTL1 providing beneficial intrinsic structural selectivity.

While tanespimycin and entacapone could be identified as METTL1 binders during FP- and ITC experiments, these two hit compounds showed only weak inhibition of the heterodimeric METTL1/WDR4 complex in the presence of ^{3}H-SAM and tRNA substrates (Figure 5F) limiting their use as potential drug discovery starting points. This is presum-

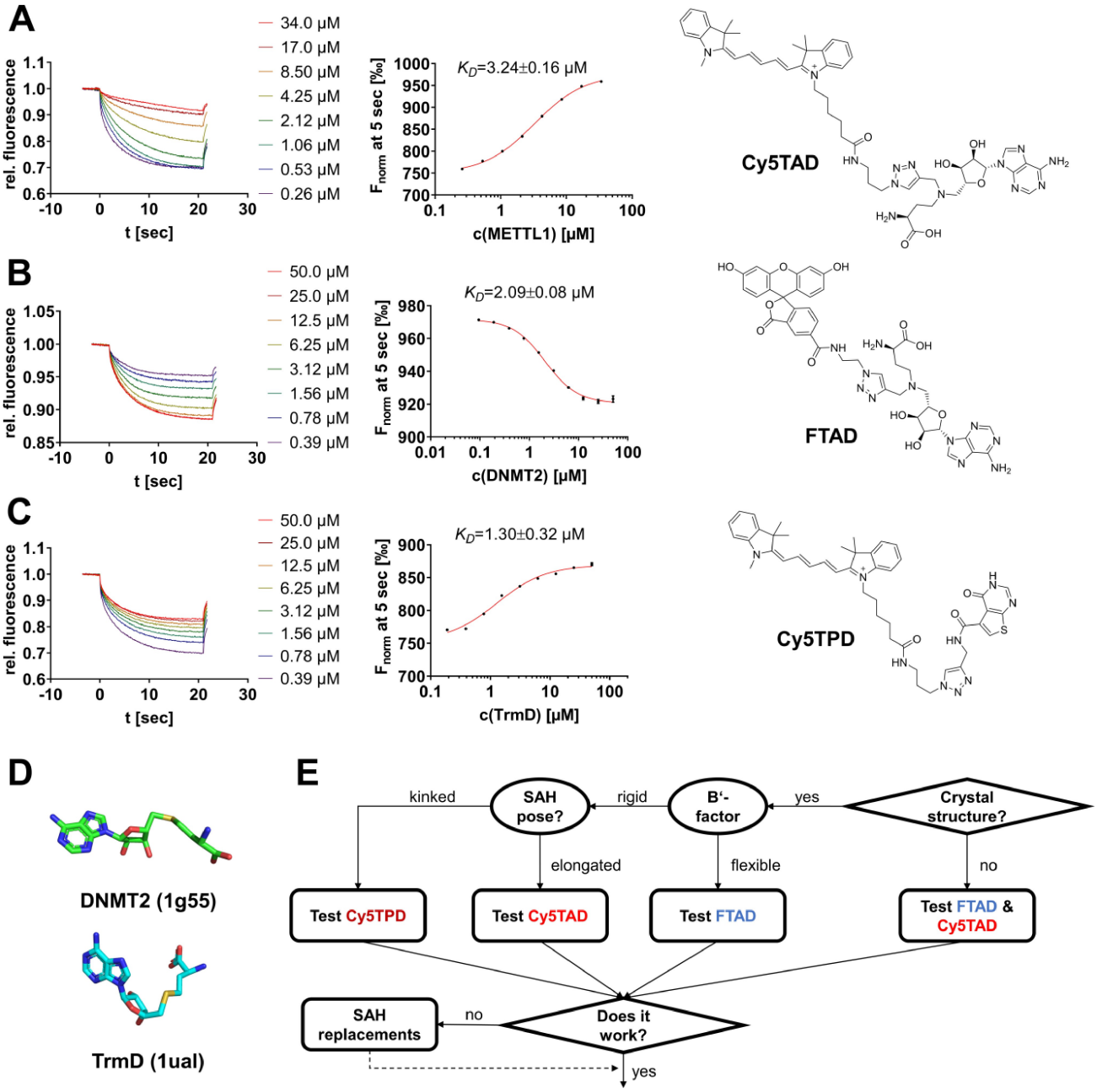

Figure 4. Validation of fluorescent MTase probes. (**A**) Validation of the HPLC-purified **Cy5TAD** probe (10 nM) with METTL1 by MST assays (mean ± SD, $n = 3$). (**B**) **FTAD** probe (100 nM) with DNMT2 (mean ± SD, $n = 3$). (**C**) **Cy5TPD** probe (10 nM) with TrmD (mean ± SD, $n = 3$). (**D**) Two distinct binding modes of SAH in MTases: DNMT2 binds SAH in an elongated mode, while TrmD shows a characteristically kinked SAH ligand. PDB-ID in brackets. (**E**) Decision tree for the choice of a probe based on the SAH conformation and MTase flexibility. The active site flexibility (B'-factors) was determined by the BANΔIT web toolkit.[21] See Table S1 for details.

ably due to the fact these hit compounds bind either to the protein-protein interaction interface or to the tRNA binding site, which is occupied in the presence of WDR4.[24] The complete METTL1 HTS assay data with the identification of additional hits can be found in the SI.

Lastly, we would like to outline the limitations of our approach described here. A general limitation of competition probe-based assays compared to label-free methods (e.g., SPR or ITC) is that inhibitors with K_D values more than one order of magnitude better than the probe affinity can only be extrapolated because of enzyme inhibitor tight-binding.[25] To illustrate this limitation and to guide a mitigation strategy, we characterized the high-affinity METTL3/14 inhibitor STM2457 ($IC_{50} = 5$ nM)[8] using the **FTAD** probe, which resulted in a tight-binding behavior ([E] = 1 µM), and thus, an apparent K_D at half-enzyme concentration of 500 nM (Figure S3G). Yet, we could overcome this limitation by synthesizing a novel high-affinity

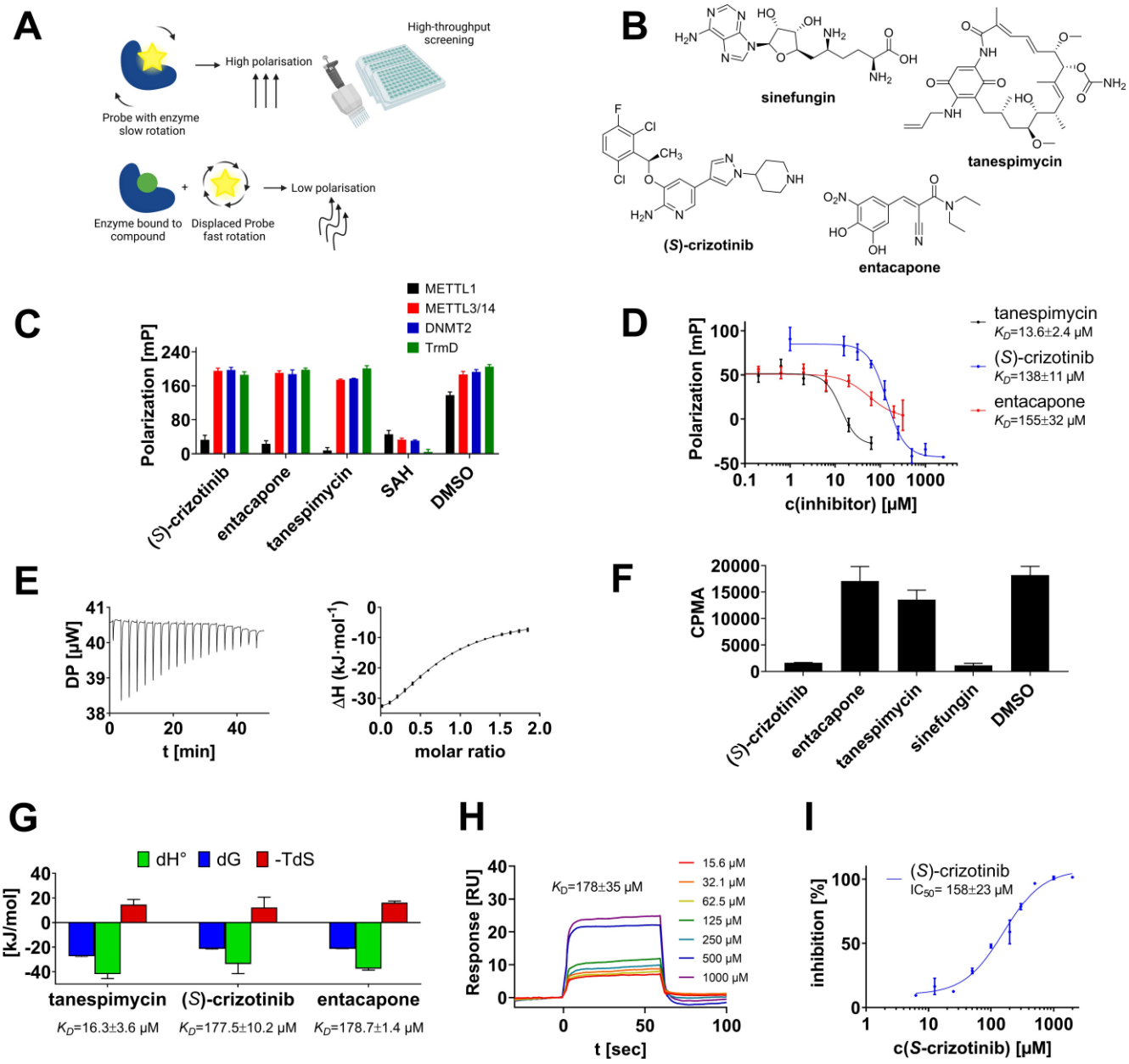

Figure 5. Using **Cy5TAD** for a high-throughput drug screening on METTL1. (**A**) Schematic depiction of the METTL1 FP screening assay. (**B**) Chemical structures of the identified METTL1 HTS-hits and positive control sinefungin. (**C**) Binding selectivity determined by FP assays against various recombinantly expressed MTases and 200 µM of the respective hit compound (mean ± SD, $n = 3$). (**D**) Dose-response curves and K_D determination by METTL1 FP assays (mean ± SD, $n = 3$). (**E**) ITC thermogram and stoichiometry plot of tanespimycin (250 µM) titrated to METTL1 (25 µM). (**F**) Screening of hit compounds (500 µM) by METTL1/WDR4 inhibition ^{3}H scintillation assays (mean ± SD, $n = 3$). Only (*S*)-crizotinib and the pan-MTase inhibitor sinefungin inhibited the METTL1/WDR4 MTase activity (CPMA). (**G**) Signature plots summarizing the ITC binding thermodynamics of all HTS hits (mean ± SD, $n = 3$). (*S*)-crizotinib and entacapone were determined by ITC displacement titrations (details in the SI).[22] Additional thermograms and stoichiometry plots can be found in Figure S6. (**H**) Determination of (*S*)-crizotinib vs. METTL1 binding affinity by SPR. Sensorgrams of triplicates and dose-response curves can be found in the Figure S9. (**I**) Dose-response curve for the ^{3}H-based IC_{50} determination of (*S*)-crizotinib inhibiting the METTL1/WDR4 complex (mean ± SD, $n = 3$).

FAM-labeled STM2457-probe (**STM-FL**, $K_D = 19$ nM) which allowed the determination of a literature-agreeing binding affinity for STM2457 with a K_D of 9.9 nM (Figure S8). This mitigation procedure might be used as a common guide for future MTase probe development: for de novo probe development the decision tree in Figure 4E is suitable for probe development, while well-known high-affinity MTase ligands offer the opportunity to decorate them directly with a fluorophore.

In addition to the identification of the highlighted probe candidates, the outlined development protocol is scalable for subsequent probe development campaigns and community researchers should expect 2–3 weeks from nanoscale synthesis to preparative validation of a probe candidate. To

share the output of this study widely, the probes are available upon request: https://ak-barthels.pharmazie.uni-mainz.de/probes-request.

Acknowledgements

Financial support by the German Research Foundation (DFG) in the framework of the Transregio Collaborative Research Center RMAP (TRR319 RMaP) is gratefully acknowledged. We would like to thank Prof. Craig Crews who generously enabled us to perform SPR experiments with his device. The Figures were created with https://www.biorender.com/ assisted by Dr. Klein. Open Access funding enabled and organized by Projekt DEAL.

Conflict of Interest

The authors declare no conflict of interest.

Data Availability Statement

The data that support the findings of this study are available in the supplementary material of this article.

Keywords: Drug discovery · Fluorescent probes · RNA

[1] M. Schwickert, T. R. Fischer, R. A. Zimmermann, S. N. Hoba, J. L. Meidner, M. Weber, M. Weber, M. M. Stark, J. Koch, N. Jung, C. Kersten, M. Windbergs, F. Lyko, M. Helm, T. Schirmeister, *J. Med. Chem.* **2022**, *65*, 9750–9788.
[2] P. Gehrtz, S. Marom, M. Bührmann, J. Hardick, S. Kleinbölting, A. Shraga, C. Dubiella, R. Gabizon, J. N. Wiese, M. P. Müller, G. Cohen, I. Babaev, K. Shurrush, L. Avram, E. Resnick, H. Barr, D. Rauh, N. London, *J. Med. Chem.* **2022**, *65*, 10341–10356.
[3] P. A. Boriack-Sjodin, S. Ribich, R. A. Copeland, *Nat. Rev. Drug Discovery* **2018**, *17*, 435–453.
[4] N. Jonkhout, J. Tran, M. A. Smith, N. Schonrock, J. S. Mattick, E. M. Novoa, *RNA* **2017**, *23*, 1754–1769.
[5] A. Cayir, *WIREs RNA* **2022**, *13*, e1702.
[6] Y. Ofir-Rosenfeld, L. Vasiliauskaitė, C. Saunders, A. Sapetschnig, G. Tsagkogeorga, M. Albertella, M. Carkill, J. Self-Fordham, J. B. Holz, O. Rausch, *Eur. J. Cancer* **2022**, *174*, S123.
[7] F. Nai, M. P. Flores Espinoza, A. Invernizzi, P. A. Vargas-Rosales, O. Bobileva, M. Herok, and A. Caflisch, *ACS Bio & Med Chem Au* **2024**, *4*, 100–110.
[8] E. Yankova, W. Blackaby, M. Albertella, J. Rak, E. De Braekeleer, G. Tsagkogeorga, E. S. Pilka, D. Aspris, D. Leggate, A. G. Hendrick, N. A. Webster, B. Andrews, R. Fosbeary, P. Guest, N. Irigoyen, M. Eleftheriou, M. Gozdecka, J. M. L. Dias, A. J. Bannister, B. Vick, I. Jeremias, G. S. Vassiliou, O. Rausch, K. Tzelepis, T. Kouzarides, *Nature* **2021**, *593*, 597–601.
[9] Y. Tao, J. G. Felber, Z. Zou, E. Njomen, J. R. Remsberg, D. Ogasawara, C. Ye, B. Melillo, S. L. Schreiber, C. He, D. Remillard, B. F. Cravatt, *Angew. Chem. Int. Ed.* **2023**, *62*, e202311924.
[10] P. J. Hill, A. Abibi, R. Albert, B. Andrews, M. M. Gagnon, N. Gao, T. Grebe, L. I. Hajec, J. Huang, S. Livchak, S. D. Lahiri, D. C. McKinney, J. Thresher, H. Wang, N. Olivier, E. T. Buurman, *J. Med. Chem.* **2013**, *56*, 7278–7288.
[11] N. L. Inniss, J. Kozic, F. Li, M. Rosas-Lemus, G. Minasov, J. Rybáček, Y. Zhu, R. Pohl, L. Shuvalova, L. Rulíšek, J. S. Brunzelle, L. Bednárová, M. Štefek, J. M. Kormaník, E. Andris, J. Šebestík, A. S. M. Li, P. J. Brown, U. Schmitz, K. Saikatendu, E. Chang, R. Nencka, M. Vedadi, K. J. F. Satchell, *ACS Infect. Dis.* **2023**, *9*, 1918–1931.
[12] J.-P. Renaud, C. Chung, U. H. Danielson, U. Egner, M. Hennig, R. E. Hubbard, H. Nar, *Nat. Rev. Drug Discovery* **2016**, *15*, 679–698.
[13] T. R. Fischer, L. Meidner, M. Schwickert, M. Weber, R. A. Zimmermann, C. Kersten, T. Schirmeister, M. Helm, *Nucleic Acids Res.* **2022**, gkac224.
[14] R. A. Zimmermann, M. Schwickert, J. L. Meidner, Z. Nidoieva, M. Helm, T. Schirmeister, *ACS Pharmacol. Transl. Sci.* **2022**, *5*, 1079–1085.
[15] T.-R. Chern, L. Liu, E. Petrunak, J. A. Stuckey, M. Wang, D. Bernard, H. Zhou, S. Lee, Y. Dou, S. Wang, *ACS Med. Chem. Lett.* **2020**, *11*, 1348–1352.
[16] J. Dowden, W. Hong, R. V. Parry, R. A. Pike, S. G. Ward, *Bioorg. Med. Chem. Lett.* **2010**, *20*, 2103–2105.
[17] G. Zhang, S. L. Richardson, Y. Mao, R. Huang, *Org. Biomol. Chem.* **2015**, *13*, 4149–4154.
[18] A. M. Rossi, C. W. Taylor, *Nat. Protoc.* **2011**, *6*, 365–387.
[19] M. Li, Z. Tao, Y. Zhao, L. Li, J. Zheng, Z. Li, X. Chen, *J. Transl. Med.* **2022**, *20*, 214.
[20] W. Cheng, A. Gao, H. Lin, W. Zhang, *Mol. Ther. Oncolytics* **2022**, *26*, 27–34.
[21] A. Dolbois, R. K. Bedi, E. Bochenkova, A. Müller, E. V. Moroz-Omori, D. Huang, A. Caflisch, *J. Med. Chem.* **2021**, *64*, 12738–12760.
[22] F. Barthels, T. Schirmeister, C. Kersten, *Mol. Inf.* **2020**, *40*, 202000144.
[23] S. J. Hammerschmidt, F. Barthels, A. C. Weldert, C. Kersten, *J. Chem. Educ.* **2024**, DOI 10.1021/acs.jchemed.3c01133.
[24] V. M. Ruiz-Arroyo, R. Raj, K. Babu, O. Onolbaatar, P. H. Roberts, Y. Nam, *Nature* **2023**, *613*, 383–390.
[25] P. J. Tonge, *ACS Infect. Dis.* **2019**, *5*, 796–808.
[26] S. Perveen, A. Khalili Yazdi, K. Devkota, F. Li, P. Ghiabi, T. Hajian, P. Loppnau, A. Bolotokova, M. Vedadi, *SLAS Discovery* **2021**, *26*, 620–627.
[27] X. Wang, J. Huang, T. Zou, P. Yin, *RNA Biol.* **2017**, *14*, 300–304.

Manuscript received: February 23, 2024
Accepted manuscript online: August 15, 2024
Version of record online: October 24, 2024